Journal of Nuclear Materials 392 (2009) 70–77

Contents lists available at ScienceDirect

Journal of Nuclear Materials

journal homepage: www.elsevier.com/locate/jnucmat

Low silicon $U(Al,Si)_3$ stabilization by Zr addition

L.M. Pizarro [a], P.R. Alonso [a,b,*], G.H. Rubiolo [a,b,c]

[a] Departamento de Materiales (GIDAT-CAC), Comisión Nacional de Energía Atómica, Avda. General Paz 1499, B1650KNA, San Martín, Pcia. Buenos Aires, Argentina
[b] Instituto Sabato, Universidad Nacional de San Martín, Avda. General Paz 1499, B1650KNA, San Martín, Pcia. Buenos Aires, Argentina
[c] Consejo Nacional de Investigaciones Científicas y Tecnológicas (CONICET), Avda Rivadavia 1917, C1033AAJ, Ciudad Autónoma de Buenos Aires, Argentina

ARTICLE INFO

Article history:
Received 1 December 2008
Accepted 22 March 2009

ABSTRACT

Previous knowledge states that $(U,Zr)Al_3$ and $U(Al,Si)_3$ phases with Zr and Si content higher than 6 at.% (7.7 wt%) and 4 at.% (1.4 wt%), respectively, does not partially transform to UAl_4 at 600 °C. In this work, four alloys within the quaternary system U–Al–Si–Zr were made with a fixed nominal 0.18 at.% (0.1 wt%) Si content in order to assess the synergetic effect of both Zr and Si alloying elements to the thermodynamic stability of the $(U,Zr)(Al,Si)_3$ phase. Heat treatments at 600 °C were undertaken and samples were analyzed by means of XRD, EPMA and EDS techniques. A remarkable conclusion is that addition of 0.3 at.% Si in the $(U,Zr)(Al,Si)_3$ phase reduces in 2.7 at.% the necessary Zr content to inhibit its transformation to $U(Al,Si)_4$.

1. Introduction

In the frame of RERTR Program (Reduced Enrichment for Research and Test Reactors) a high density uranium based fuel that could remain stable in the body cubic centered (bcc) phase during fabrication and irradiation in the reactor is being developed. Research is focused in a U–Mo alloy dispersed fuel in the aluminum matrix [1]. Although it meets most of the fuel requirements, further development of this fuel has been delayed due to an unacceptable volume expansion caused by (U–Mo)–Al interaction layer (IL) formation and a subsequent gross pore formation at the interface between U–Mo and matrix Al [2].

It has been suggested that the IL is amorphized during irradiation and the structural instability of the IL is due to its amorphous character [3]. The same authors remark that in–pile test show that an IL with a high Al-content tends to be amorphized more easily. Maintaining the interaction layer of U–Mo/Al dispersion fuel as a stable low-Al content compound such as $(U–Mo)Al_3$ appears to be the key to avoiding massive pore formation. In brief, it has been proposed that the $(U,Mo)Al_3$ compound (cP4, space group 221) should be stabilized against formation of compounds with a higher aluminum content, such as UAl_4 (oI20, space group 74).

Previous studies have tried the Si-modification of the UAl_3 fuel in the UAl_3–Al dispersion fuel to suppress UAl_4 formation during the high-temperature fabrication process [4–7]. On an analogous base, the Si-modification of the Al matrix in the U–Mo/Al dispersion fuel has been recently proposed to solve the stability of the IL [8]. Out-of-pile diffusion studies have shown that Si indeed accumulates in the IL between U–Mo and Al–Si [9,10]. In-pile tests have also shown the positive effect of Si: the IL thickness was much thinner than in the fuel plates using a pure Al matrix, and no porosity was formed [11,12].

It was also noticed that minor silicon quantities would be required to solve the stability of the IL if a fourth element is present [8]. The early U–Al fuel developers have also tried the Zr-modification of the UAl_3 fuel [7]. The experimental evidence showed that the addition of 14 wt% zirconium as a third element is enough to inhibit UAl_4 formation.

In a recent publication [13], the results of diffusion-couple tests between U–Mo–*x*Zr and Al–*y*Si alloys with various contents of Zr and Si were reported. The interaction product formed in a U–Mo–2Zr vs. Al–5Si (wt%) diffusion couple tested at 580 °C showed that the composition of the IL goes from $U(Al,Si)_2$ on the U–Mo–Zr side to $U(Al,Si)_3$ on the Al–Si side, which indicates an increased chemical potential gradient for Si with the presence of Zr in the U–Mo alloy.

Modification of the UAl_3 phase by means of simultaneous addition of silicon and zirconium in order to suppress UAl_4 formation has not been reported. We have thus decided to determine UAl_3 phase stability in U–Al–Zr–Si alloys containing 50–47 wt% uranium, 49.9–46.9 wt% aluminum, 0–6 wt% zirconium and 0.1 wt% silicon.

2. Experimental techniques

Four alloys were made from uranium 99.975%, aluminum 99.99%, silicon 99.999% and zirconium 99.7% (alloys labeled 0, 1, 3 and 6 in Table 1). Special attention was paid to the silicon and

* Corresponding author. Address: Departamento de Materiales (GIDAT-CAC), Comisión Nacional de Energía Atómica, Avda. General Paz 1499, B1650KNA, San Martín, Pcia. Buenos Aires, Argentina. Tel.: +54 11 6772 7247; fax +54 11 6772 7362.
E-mail address: pralonso@cnea.gov.ar (P.R. Alonso).

0022-3115/$ - see front matter © 2009 Elsevier B.V. All rights reserved.
doi:10.1016/j.jnucmat.2009.03.052

Table 1
Alloys compositions.

Sample	U (wt%/at.%)	Al (wt%/at.%)	Si (wt%/at.%)	Zr (wt%/at.%)
0	50.00/10.18	49.90/89.65	0.1/0.17	0/0.00
1	49.47/10.12	49.43/89.18	0.1/0.17	1/0.53
3	48.48/10.01	48.42/88.20	0.1/0.18	3/1.62
6	47.00/9.85	46.90/86.69	0.1/0.18	6/3.28

zirconium content in raw materials as minor quantities of these two elements could influence the results of the present work. High purity aluminum and silicon were used. Thus, only zirconium and uranium were inspected for impurities (see Appendix A for details of composition). Si content in Zr is <0.001 wt% (10 wt ppm) as indicated by chemical analysis. Si content in uranium was measured as 0.0024 wt% (24 wt ppm). No zirconium content was evident in the uranium analysis. Total silicon or zirconium content as impurity was thus negligible when compared with the desired content 0.1 wt% Si and 0, 1, 3, 6 wt% Zr in the alloys.

Alloys compositions were designed taking into account the liquidus projection into the ternary U–Al–Zr system [14] as a basis for the estimation of the solidification path in the quaternary U–Al–Zr–Si system. In this way, we aimed for UAl_3 as primary phase avoiding the formation of UAl_2. Then, the range 35–56 wt% U and 0–9 wt% Zr was identified. After Boucher's work [4] it is known that a content of 0.1 till 0.6 wt% Si in a U–Al alloy with 35 wt% U is not enough to inhibit UAl_4 formation from $U(Al,Si)_3$ at 600 °C, though time required for transformation increases with silicon content. In order to test increasing amounts of Zr addition to suppress the reaction between Al and primary $(U,Zr)(Al,Si)_3$ to form UAl_4 after solidification, the silicon content has to be the smallest possible compatible with a measurable treatment time. From these considerations 0.1 wt% Si content was chosen for all the alloys in this study.

A non-consumable tungsten electrode arc furnace was employed to melt the pure components and produce the alloys under a controlled argon atmosphere using a water-refrigerated copper crucible and an oxygen titanium getter. The alloys were melted and remelted at least four times to ensure homogeneity.

Heat treatments at 600 °C were made during 1000 h. The heat-treated specimens were wrapped in tantalum foils and sealed in silica tubes under argon atmosphere to protect them from contamination during the heat treatments. Finally, they were water-quenched to room temperature without breaking the containers.

Metallographic techniques and composition measurements were employed to identify the different phases. Microstructural analysis using a PHILIPS PSEM-500 scanning electron microscope (SEM) was performed and both secondary and backscattered electron images were taken. Elemental compositions were obtained with Energy Dispersive Spectroscopy (EDS) in the same device. Local concentrations of aluminum, uranium and zirconium were determined with electron-probe microanalysis (EPMA) in a Cameca SX50 device fitted with a wavelength-dispersive spectrometer.

X-ray diffraction (XRD) techniques in a PW3710 BASED PHILIPS device employing Cu-Kα_1 and Kα_2 radiation at room temperature were used to study the stability of the $(U,Zr)(Al,Si)_3$ phase after the annealing test. A scan of the various diffraction peaks in the 10–120° (2θ) range was recorded to determine the lattice parameters of the phases involved in this work. The used step size was 0.03° (2θ), measuring a total of 10 s per step. All possible reflections for a given lattice dimension and symmetry were generated for each probable phase in the specimen using the PowderCell 2.4 software [15]. This list of possible reflections was compared to the observed peak positions in the experimental profile and those with a high intensity peak to background ratio were identified with a phase and reflection plane. The final lattice parameters of a phase and its errors were then calculated, using the mean square method, from the *d*-spacing of identified peaks in the experimental profile.

Prior to metallographic observations, the samples were grounded on silicon carbide paper, polished with diamond paste (1 μm) and electrolytically polished at 20 V during 10 s using a

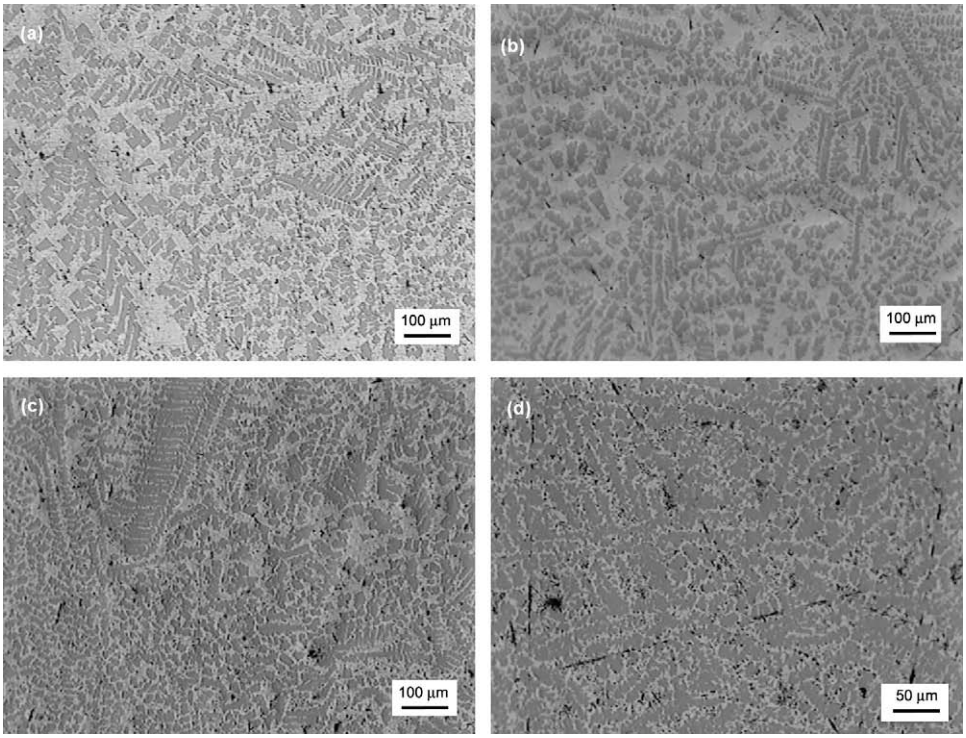

Fig. 1. Optical micrographs of as-cast alloys. (a) Sample 0, (b) sample 1, (c) sample 3 and (d) sample 6.

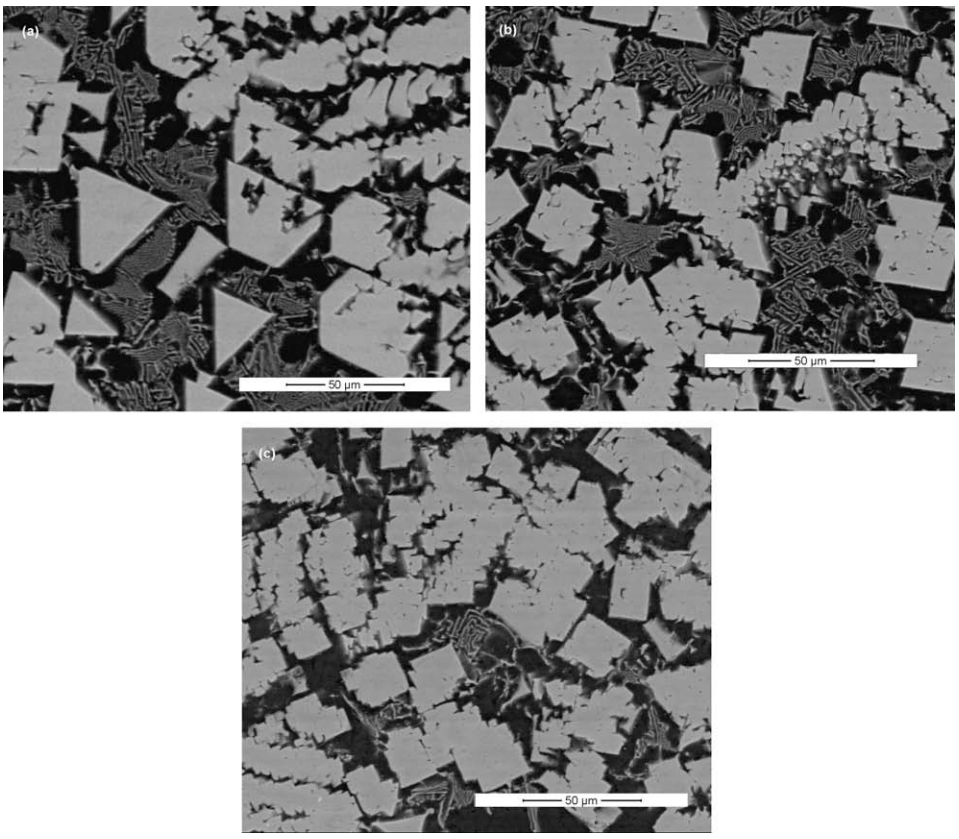

Fig. 2. Secondary electron images of the as-cast: (a) sample 1, (b) sample 3 and (c) sample 6 alloy microstructures. Presence of primary phase and eutectic-type zones is evident.

solution of phosphoric acid, ethylic alcohol, distilled water and 2-*n*-butoxiethanol at volume ratio 54:21.6:2.8:21.6. XRD samples were free from electrolytic polishing in order to exhibit a plane surface.

3. Results and discussion

3.1. As-cast alloys

Metallographic examination of as-cast alloys revealed a primary phase surrounded by a eutectic-type component. The dendrite morphology of the primary phase is observed in Fig. 1 while the eutectic morphology is clearly shown by the SEM secondary electron images of Fig. 2.

Elemental composition obtained by EDS confirms that the primary phase contains Zr, but this is not detected in the eutectic even if a 5×5 μm area were used for an integrated measurement.

The XRD patterns of as-cast alloys (Fig. 3) show the UAl_3, UAl_4 and Al phases; in the alloy 6 no UAl_4 could be detected. The lattice parameter of UAl_3 phase shows a tendency to diminish with increasing zirconium content, while lattice parameters belonging to UAl_4 and Al phase are invariant (Table 2). These facts are seen as an evidence of Zr solubility in the UAl_3 phase and not in UAl_4. Based on interpolation of lattice parameter of $U(Al,Si)_3$ measurements reported by Dwight [16], a negligible variation of the UAl_3 lattice parameter with the addition of a small quantity of silicon can be expected. This could lead to an estimation for zirconium

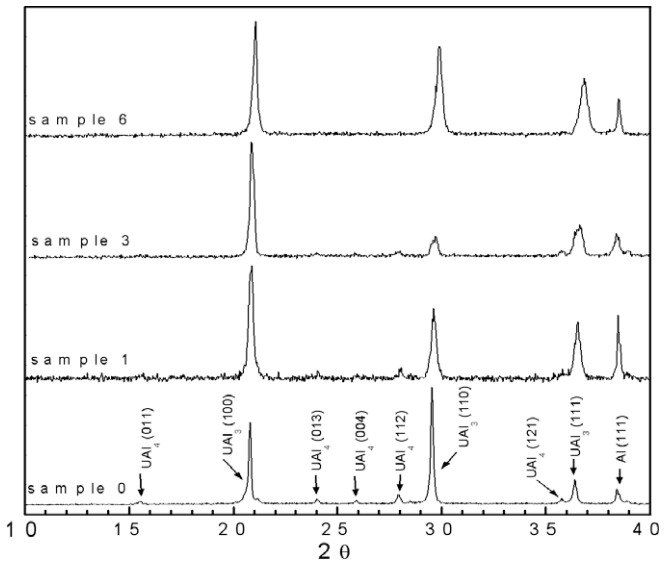

Fig. 3. X-ray diffraction patterns of as-cast alloys.

Table 2
Lattice parameters of observed phases and zirconium content in $(U,Zr)(Al,Si)_3$ phase calculated from experimental X-rays diffraction patterns in as-cast alloys.

Sample	Lattice parameter (nm) ($\pm 5 \cdot 10^{(-4)}$ nm)			Zr content (at.%)
	UAl_3	UAl_4	Al	
0	0.427	$a = 0.440$ $b = 0.625$ $c = 1.373$	0.405	0
1	0.426	$a = 0.440$ $b = 0.625$ $c = 1.373$	0.405	(1.4 ± 0.7)
3	0.425	$a = 0.440$ $b = 0.625$ $c = 1.373$	0.405	(2.8 ± 0.7)
6	0.422	–	0.405	(6.9 ± 0.7)

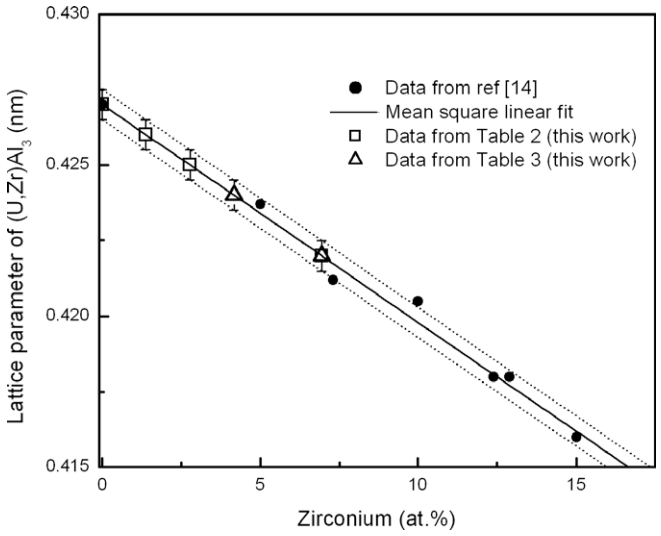

Fig. 4. Lattice constant of the $(U,Zr)Al_3$ phase with increasing Zr content. Close symbols indicate measurements on single phases samples from reference [14]. The solid line is a mean square linear fit between 0 and 15 at.% Zr. Open symbols are the predicted Zr content of our XRD results in Tables 2 and 3. Dashed lines enclose the confidence limit for the Zr content in the $(U,Zr)Al_3$ phase as obtained from the errors in their measured lattice constants.

content in the $(U,Zr)(Al,Si)_3$ phase by means of our XRD results and the calibration curve shown in Fig. 4 (also see Table 2).

We have used the ternary U–Al–Zr liquidus diagram of Ref. [14] and SEM images of as-cast alloys (Fig. 2) as a basis for the analysis of the solidification path in the quaternary U–Al–Zr–Si [17]. Solidification path is schematically shown in Fig. 5(a) and (b). In all alloys, the content of Zr in the primary phase is high and has a similar increasing trend as the Zr content in the global composition of the alloys. Liquid becomes poorer in U and Zr till it reaches the univariant reaction Liquid → Al(Si) + $(U,Zr)(Al,Si)_3$. A eutectic type structure of both phases Al(Si) + $(U,Zr)(Al,Si)_3$ is precipitated as the liquid reaches the eutectic invariant point (E) Liquid → Al(Si) + $(U,Zr)(Al,Si)_3$ + $U(Al,Si)_4$. Fig. 6(a) and (b) clearly shows the three stages of solidification. The two-phase eutectic-type Al(Si) + $(U,Zr)(Al,Si)_3$ coexists with the primary phase. Some precipitates evidence continuity with the primary phase and can be identified as the same structure. The final three-phase eutectic is distinguished as a finer structure. The conodal connecting the estimated $(U,Zr)Al_3$ phase composition and the global composition of the alloy in the liquidus diagram of Ref [14] (see also Fig. 5) predicts a zirconium content of about 0.3 at.% for the eutectic component in all analyzed alloys.

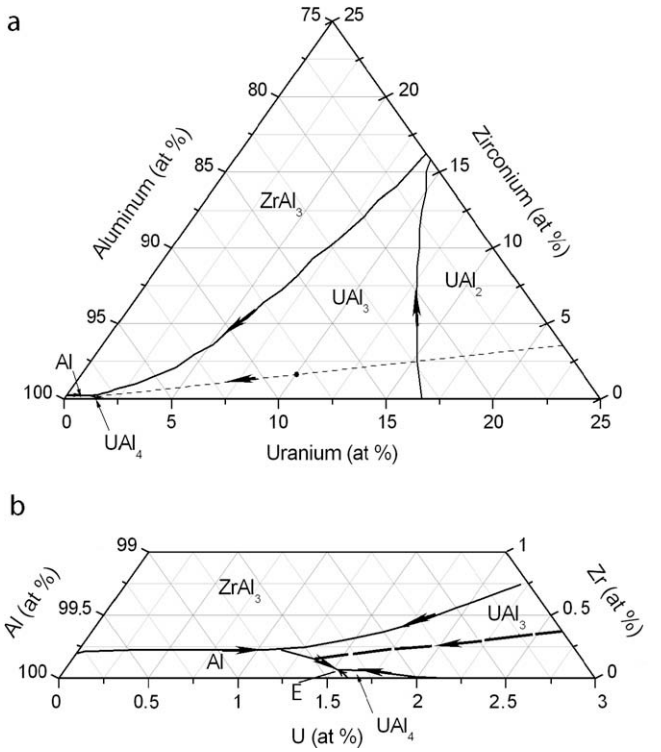

Fig. 5. Schematic solidification path for alloy 3 drawn on partial liquidus projection from Ref. [14]. Primary solidification phases are shown. (a) 0 < at.% U < 25. The circle denotes the global alloy composition. (b) 0 < at.% U < 3, 0 < at.% Zr < 1.

In conclusion, the as-cast alloys in this work show a solidification microstructure comprising a primary phase $(U,Zr)(Al,Si)_3$, a eutectic two-phase component Al(Si) + $(U,Zr)(Al,Si)_3$ and a eutectic three-phase component Al(Si) + $(U,Zr)(Al,Si)_3$ + $U(Al,Si)_4$. In the last two components, the amount of Zr involved is less than 0.3 at.% and then not detectable by EDS.

3.2. Annealed alloys

After the heat treatment, the sharp corners of the primary phase were rounded off. This effect on the lamellar structure of eutectic components forms small spheroid precipitates (Fig. 7).

All the heat treated samples showed the presence of $U(Al,Si)_4$ in the XRD pattern, decreasing in amount with increasing zirconium content (Fig. 8) and being hardly noticeable in sample 6. In Table 3 we summarize the lattice parameters of the phases. The lattice parameter of the $(U,Zr)(Al,Si)_3$ phase diminished after the anneal-

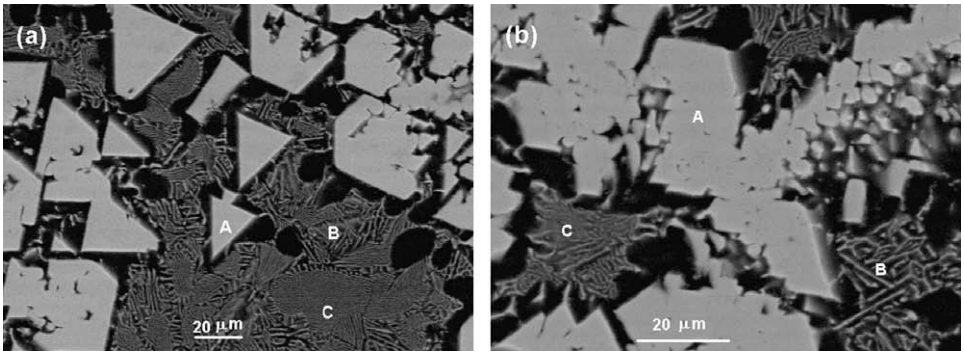

Fig. 6. Secondary electron images of the eutectic-type areas into the as-cast: (a) sample 1 and (b) sample 3 alloy microstructures. **A** is the $(U,Zr)(Al,Si)_3$ primary phase, **B** is the univariant eutectic-type zone $(U,Zr)(Al,Si)_3$ + Al and **C** is the final eutectic $(U,Zr)(Al,Si)_3$ + Al(Si) + $U(Al,Si)_4$.

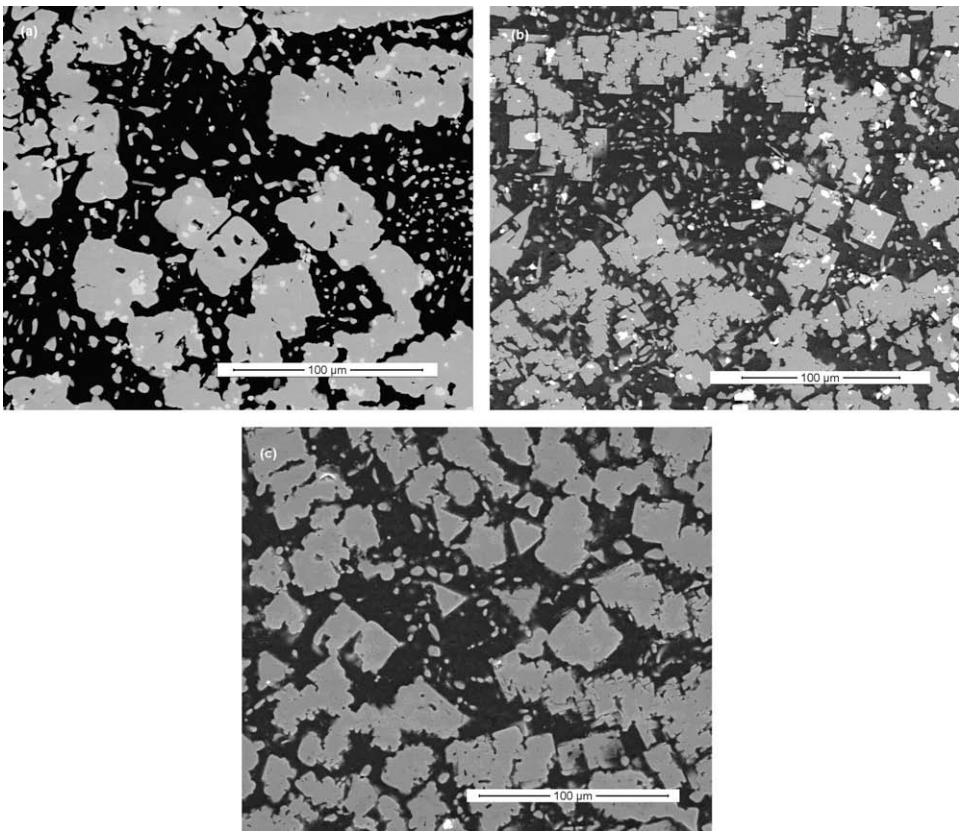

Fig. 7. Secondary electron images of the annealed: (a) sample 1, (b) sample 3 and (c) sample 6 alloy microstructures. The darkest regions contain Al(Si) and Al(Si) + $(U,Zr)(Al,Si)_3$ + $U(Al,Si)_4$ eutectic. The brightest contrast phases are $(U,Zr)(Al,Si)_3$. The lamellar structure of eutectic components is transforming into small spheroid precipitates.

ing in samples 1 and 3 while it remained constant in sample 6. The lattice parameters belonging to the $U(Al,Si)_4$ and Al(Si) phases are invariant during the annealing.

Zirconium content is not detectable in the small spheroid precipitates within the eutectic zone by EDS composition measurements.

EPMA measurements were performed over the heat treated samples. The procedure consisted in obtaining one punctual measurement every 2 μm along a 100 μm line across dendritic arms of the primary phase and the matrix including the small spheroid precipitates (Fig. 7). Thus, a dispersion of data is obtained since measurements involve phases as well as interphases. The complete set of composition values obtained was renormalized so as to consider only the U, Al and Zr content and plotted in Fig. 9 on the ternary phase diagram U–Al–Zr from Ref. [14] at 600 °C. In the same diagram two-phase and three-phase fields involving Al(Si), $U(Al,Si)_4$ and $(U,Zr)(Al,Si)_3$ are depicted according to compositions from Ref [14]. We consider the U–Al–Zr phase diagram to be representative of the quaternary diagram as all samples have the same Si content, which is small enough to consider that the quaternary diagram will exhibit the same phases that appear in the ternary diagram though with slights changes in composition.

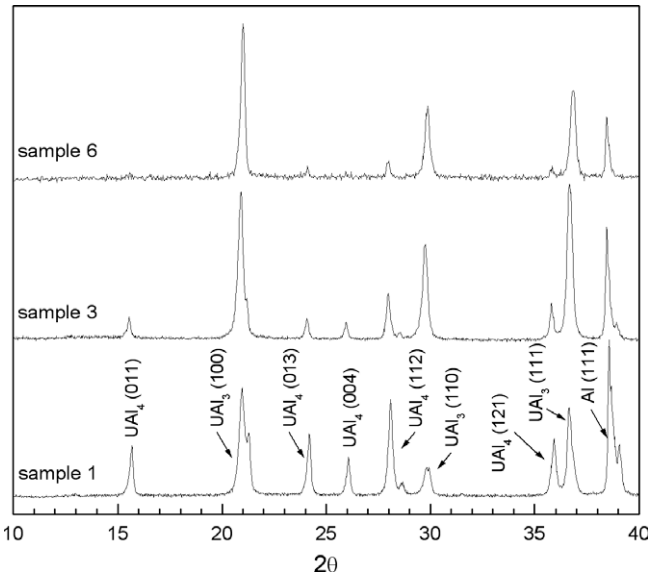

Fig. 8. X-ray diffraction patterns of annealed alloys.

Measurements on alloy 3 (Fig. 9(b)) give values for compositions of the three phases Al(Si), $U(Al,Si)_4$ and $(U,Zr)(Al,Si)_3$. Moreover, there are measurements involving the three possible interphases, being $Al(Si)/U(Al,Si)_4$; $U(Al,Si)_4/(U,Zr)(Al,Si)_3$ and $Al(Si)/(U,Zr)(Al,Si)_3$. Scheme in Fig. 10(a) depicts the morphology of the phases structure according to these results. The $(U,Zr)(Al,Si)_3$ primary phase transforms to $U(Al,Si)_4$ throughout its periphery, while the $(U,Zr)(Al,Si)_3$ precipitates emerging from the univariant reaction do not transform due to their higher Zr content. Dispersion of measurements thus results in a delimitation of the three-phase region Al(Si) + $U(Al,Si)_4$ + $(U,Zr)(Al,Si)_3$.

Keeping this analysis in mind, results from measurements on alloy 1 (Fig. 9(a)) can be understood as depicted in Fig. 10(b). The interphase $Al(Si)/(U,Zr)(Al,Si)_3$ is not found since the $(U,Zr)(Al,Si)_3$ precipitates formed during the univariant reaction transform to $U(Al,Si)_4$ throughout its periphery so abundantly that the $(U,Zr)(Al,Si)_3$ phase cannot be measured alone.

Measurements trends in alloy 6 (Fig. 9(c)) fail to exhibit the interphase $(U,Zr)(Al,Si)_3/U(Al,Si)_4$. This is because the primary phase $(U,Zr)(Al,Si)_3$ as well as the $(U,Zr)(Al,Si)_3$ precipitates formed during the univariant reaction have already a Zr content close to the equilibrium one and does not transform to $U(Al,Si)_4$. The $U(Al,Si)_4$ measured in this sample comes from the precipitates involved in the final eutectic three-phase component.

Finally, two-phase and three-phase fields are established in the equilibrium phase diagram. Measurements in the heat treated samples from alloys 1 and 3 lie within the three-phase region Al(Si) + $U(Al,Si)_4$ + $(U,Zr)(Al,Si)_3$, while the heat treated sample from alloy 6 belongs to the two-phase region Al(Si) + $(U,Zr)(Al,Si)_3$.

We can now account for the silicon contents in the various phases. A plot of zirconium and silicon content in heat treated samples 1, 3 and 6 versus distance along a line across the dendritic arms and the matrix can be found in Fig. 11(a)–(c). It can be noted that the compositional profile of both elements shows an oscillation along the line, increasing or lowering its respective content values in phase. Since zirconium was mainly found in the $(U,Zr)(Al,Si)_3$ phase, as it was concluded from the analysis of the pseudo-ternary equilibria of Fig. 9, this effect can be seen as an evidence of mutual solubility of Si and Zr in the $(U,Zr)(Al,Si)_3$ phase.

This analysis is in keeping with the results from XRD shown in Table 3, where it can be observed that the estimation for zirconium content in the $(U,Zr)(Al,Si)_3$ phase by means of our XRD results and the calibration curve (Fig. 4) compare well with those of the composition measurements by EPMA. An agreement within experimental uncertainty is found. Estimations from XRD

Table 3
Lattice parameters of observed phases and $(U,Zr)Al_3$ composition in annealed alloys. EPMA and XRD measurements.

Sample	Lattice parameter (nm) ($\pm 5 \cdot 10^{(-4)}$ nm)			$(U,Zr)(Al,Si)_3$	
	$(U,Zr)(Al,Si)_3$	$U(Al,Si)_4$	Al(Si)	XRD Zr content (at.%)	EPMA Composition (at.%)
1	0.424	$a = 0.440$	0.405	(4.2 ± 0.7)	–
3	0.424	$b = 0.625$		(4.2 ± 0.7)	(74.9 ± 0.7)Al
		$c = 1.373$			(21.5 ± 0.6)U
					(3.3 ± 0.4)Zr
					(0.30 ± 0.01)Si
6	0.422			(6.9 ± 0.7)	(76.1 ± 0.2)Al
					(16.9 ± 0.9)U
					(6.8 ± 0.9)Zr
					(0.20 ± 0.08)Si

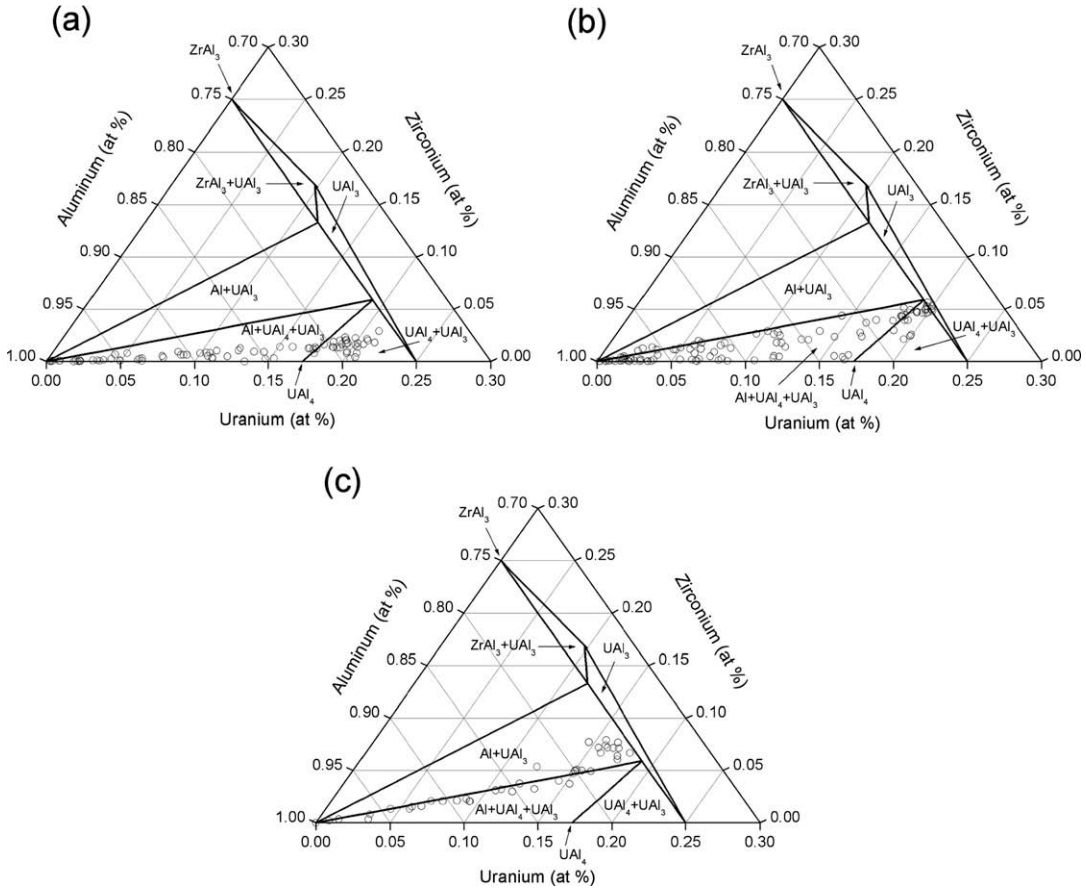

Fig. 9. Composition measurements (EPMA) in the heat treated alloys: (a) sample 1, (b) sample 3 and (c) sample 6. Quaternary compositions are renormalized to be superimposed in the aluminum rich corner of the ternary Al–Zr–U equilibrium phase diagram at 600 °C from Ref. [14]. $(U,Zr)(Al,Si)_3$ is denoted as its terminal phase name UAl_3.

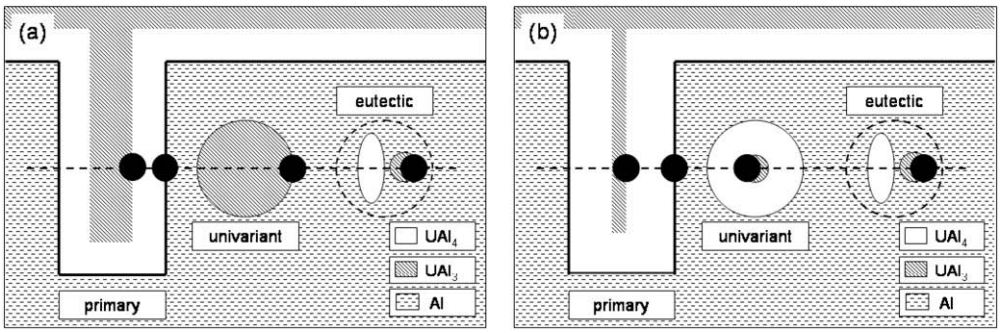

Fig. 10. Schematic depiction of phase's morphology in the heat treated alloys showing the diameter of the electron beam (dark circle) in relation to the size of phases and interphases. (a) Sample 3 and (b) sample 1.

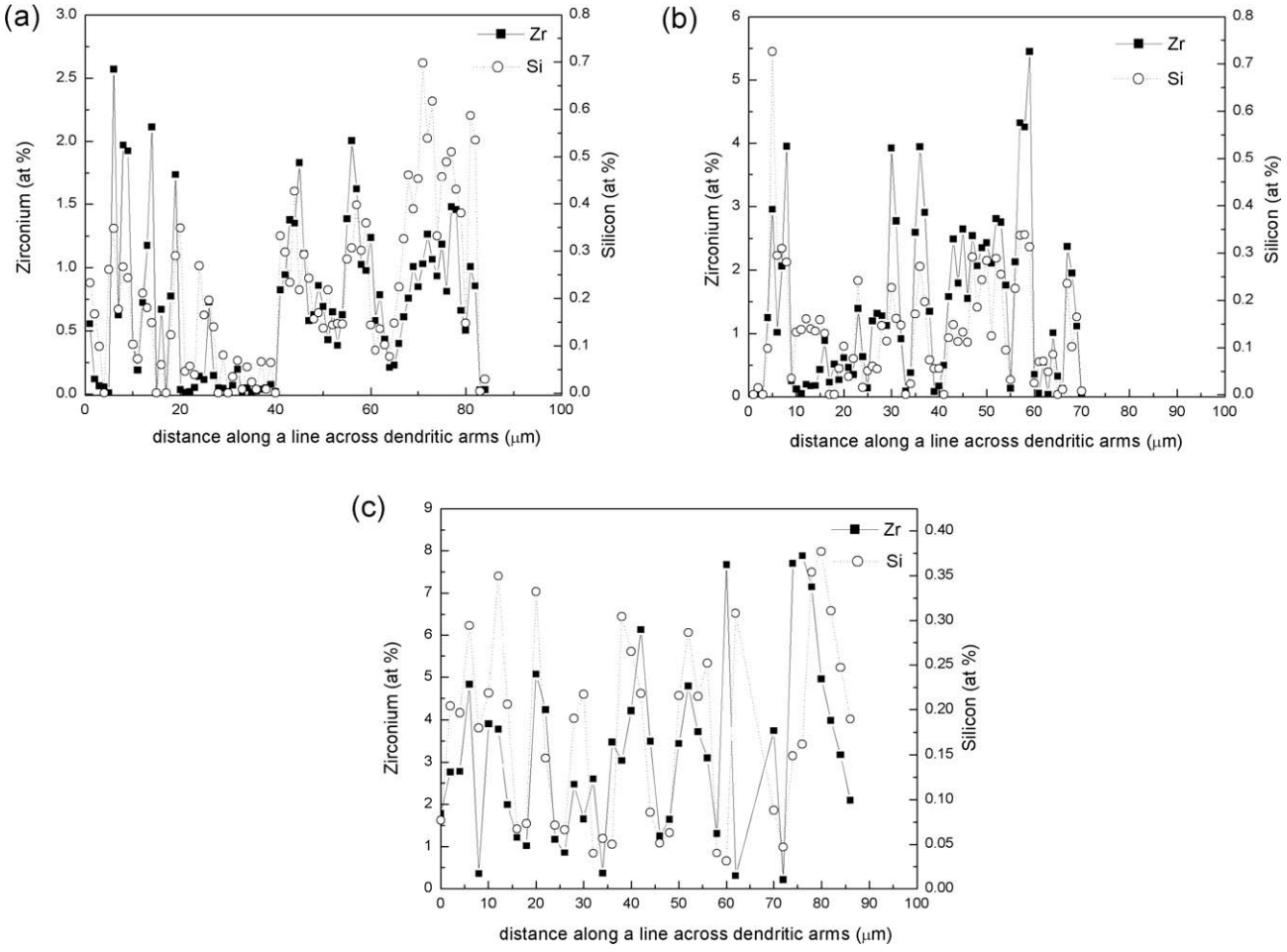

Fig. 11. Zirconium and silicon composition profile along a line across the dendritic arms and the matrix in the heat treated alloys. (a) Sample 1, (b) sample 3 and (c) sample 6.

Table A1
Impurity content of Zr (wt ppm) by chemical analysis.

Al	B	C	Ca	Cd	Cl	Co	Cr	Cu	Fe	H	Hf
<20	<0.25	27–34	<10	<0.25	<5	<10	<50	<10	105–170	<3	69–105
Mg	Mn	Mo	N	Na	Nb	Ni	O	P	Pb	Si	Sn
<10	<25	<10	<20	<5	<50	<35	400–440	<3	<25	<10	<10
Ta	Ti	U	V	W							
<50	<25	<1	<25	<25							

Table A2
Impurity content of U (wt ppm) by spectrographic analysis.

Al	Mn	Cr	Fe	Mo	Mg	Cu	Si	Ti	Co	Ni	Ca
<10	12	<4	27	<3	60	6	24	<4	<3	<6	100

confirm thermal stability of the primary phase $(U,Zr)(Al,Si)_3$ in alloy 6 with the same 7 at.% Zr content in as-cast and heat treated samples, while the $(U,Zr)(Al,Si)_3$ composition in alloys 1 and 3 evolves towards equilibrium with the heat treatment, increasing Zr content. Since the $(U,Zr)(Al,Si)_3$ phase is surrounded by the Al matrix with negligible Zr and Si content, the increment in the Zr and Si concentration is only possible by a migration of the Zr and Si atoms from the periphery towards the inner zones of the primary phase. The loss of mass is compensated by the movement of Al atoms, which causes the formation of UAl_4 in the periphery.

In order to examine the synergetic effect of both Zr and Si alloying elements on the thermodynamic stability of the UAl_3 phase, we state the following hypothesis: the enthalpy of mixing for the quaternary phase $(U,Zr)(Al,Si)_3$ in the three-phase equilibrium field $Al + U(Al,Si)_4 + (U,Zr)(Al,Si)_3$ can be estimated, at first approximation, as the composition-weighed average of the end members $(U,Zr)Al_3$ and $U(Al,Si)_3$ in the same three-phase equilibrium field. Petzow [14] reported the composition (19U 6Zr 75Al) for the $(U,Zr)Al_3$ phase in the three-phase field $Al + UAl_4 + (U,Zr)Al_3$ and Dwight [16] reported the composition (25U 71Al 4Si) for the $U(Al,Si)_3$ phase in the three-phase field $Al + UAl_4 + U(Al,Si)_3$, both at 600 °C. Then, formation energy E_F of a quaternary $(U,Zr)(Al,Si)_3$ intermediate compound should be such that:

$$E_F(C_U U\ C_{Zr} Zr\ C_{Al} Al\ C_{Si} Si) = t\ E_F(19U\ 6Zr\ 75Al) + (1-t)E_F(25U\ 71Al\ 4Si),$$

where C_x stands for composition of element X and $0 < t < 1$.

Solving this equation for the silicon and zirconium compositions in at.%, C_{Si} and C_{Zr}, we have:

$$C_{Si} = 4 - \frac{2}{3} C_{Zr}.$$

Our result of (74.9Al 21.5U 3.3Zr 0.3Si) for the $(U,Zr)(Al,Si)_3$ in the three-phase field $Al(Si) + U(Al,Si)_4 + (U,Zr)(Al,Si)_3$ gives $C_{Si} = 0.3 \langle\langle 4 - \frac{2}{3} 3.3 = 1.8$. This means that a lower content of silicon than the one predicted in the interpolation is needed to stabilize $(U,Zr)(Al,SI)_3$ against the $U(Al,Si)_4$ compound. The Zr and Si bonds thus play a significant role in the reduction of the enthalpy of mixing in the compound $(U,Zr)(Al,Si)_3$. This finding is also in agreement with the presence of several line compounds in the binary Zr–Si phase diagram [18].

4. Conclusions

According to previous knowledge the ternary $(U,Zr)Al_3$ and $U(Al,Si)_3$ phases do not partially transform to UAl_4 at 600 °C when Zr and Si content is higher than 6 at.% (7.7 wt%) and 4 at.% (1.4 wt%), respectively. Our analysis of samples of the quaternary U–Al–Zr–Si alloys stabilized for 1000 h at 600 °C reveals that the necessary Zr and Si content to inhibit the transformation of the quaternary $(U,Zr)(Al,Si)_3$ to UAl_4 can be reached with the combination of 3.3 at.% Zr and 0.3 at.% Si. This pair of values does not comply with the relationship $C_{Si} = 4 - \frac{2}{3} C_{Zr}$ predicted for the ideal mixing of the $(U,Zr)Al_3$ and $U(Al,Si)_3$ phases, thus showing that the Zr and Si bonds play a significant role in the reduction of the enthalpy of mixing in the compound $(U,Zr)(Al,Si)_3$.

Aknowledgements

This work was partially supported by the Secretaría de Ciencia y Tecnología del Gobierno Argentino under Grant BID 1201/OC-AR PICT N° 12-11186 (program 2004–2007) and by the Universidad Nacional de San Martín under Grant C/033 (program 2004–2006).

Appendix A

See Tables A1 and A2.

References

[1] J.L. Snelgrove, G.L. Hofman, M.K. Meyer, C.L. Trybus, T.C. Wiencek, Nucl. Eng. Des. 178 (1997) 119.
[2] A. Leenaers, S. Van den Berghe, E. Koonen, C. Jarousse, F. Huet, M. Trotabas, M. Boyard, S. Guillot, L. Sannen, M. Verwerft, J. Nucl. Mater. 335 (2004) 39.
[3] H.J. Ryu, Y.S. Kim, G.L. Hofman, D.D. Keiser, in: Proceedings of the 2006 RERTR International Meeting, Cape Town, South Africa, 29 October–2 November 2006. <http://www.rertr.anl.gov>.
[4] R. Boucher, J. Nucl. Mater. 1 (1959) 13.
[5] W.C. Thurber, R.J. Beaver, Oak Ridge (USA) Report, ORNL-2602, 1959.
[6] M.L. Picklesimer, W.C. Thurber, US Patent 2950188, USPO, 1960.
[7] A.K. Chakraborty, R.S. Crouse, W.R. Martin, J. Nucl. Mater. 38 (1971) 93.
[8] Y.S. Kim, G.L. Hofman, H.J. Ryu, J. Rest, in: Proceedings of the 2005 RERTR International Meeting, Boston, USA, 6–10 November 2005. <http://www.rertr.anl.gov>.
[9] M. Mirandou, S. Arico, L. Gribaudo, S. Balart, in: Proceedings of the 2005 RERTR International Meeting, Boston, USA, 6–10 November 2005. <http://www.rertr.anl.gov>.
[10] J.M. Park, H.J. Ryu, G.G. Lee, H.S. Kim, Y.S. Lee, C.K. Kim, Y.S. Kim, G.L. Hofman, in: Proceedings of the 2005 RERTR International Meeting, Boston, USA, 6–10 November 2005. <http://www.rertr.anl.gov>.
[11] Y.S. Kim, G.L. Hofman, H.J. Ryu, M.R. Finlay, D. Wachs, in: Proceedings of the 2006 RERTR International Meeting, Cape Town, South Africa, 29 October–2 November 2006. <http://www.rertr.anl.gov>.
[12] M. Ripert, S. Dubois, P. Boulcourt, S. Naury, P. Lemoine, in: Transactions of the 10th International Topical Meeting on RRFM, ENS, Sofia, Bulgaria, 2006.
[13] J.M. Park, H.J. Ryu, S.J. Oh, D.B. Lee, C.K. Kim, Y.S. Kim, G.L. Hofman, J. Nucl. Mater. 374 (2008) 422.
[14] G. Petzow, H.E. Exner, A.K. Chakraborty, J. Nucl. Mater. 25 (1968) 1.
[15] W. Kraus, G. Nolze, J. Appl. Cryst. 29 (1996) 301.
[16] A.E. Dwight, Argonne National Laboratory Report No. ANL-82-14, Argonne, IL, 1982.
[17] L.M. Pizarro, MSc thesis, Instituto de Tecnología "Jorge Sabato", Universidad Nacional Gral. San Martín – Comisión Nacional de Energía Atómica, Argentina, 2008.
[18] T.B. Massalski, H. Okamoto, P. Subramanian, L. Kacprzak, in: Binary Alloy Phase Diagrams, 2nd Ed., ASM International, 1990.